Journal of Alloys and Compounds 509 (2011) 632–635

Contents lists available at ScienceDirect

Journal of Alloys and Compounds

journal homepage: www.elsevier.com/locate/jallcom

Isothermal section of the Ho–Co–Fe system at 773 K

Wei He*, Yunhong Zhao, Yongzhi Zhang, Meihua Yu, Lingmin Zeng

Key Laboratory of Nonferrous Metal Materials and New Processing Technology, College of Materials Science and Engineering, Ministry of Education, Guangxi University, Nanning 530004, PR China

ARTICLE INFO

Article history:
Received 3 August 2010
Received in revised form
18 September 2010
Accepted 22 September 2010
Available online 1 October 2010

Keywords:
Phase diagram
Ho–Co–Fe system
Rare earth alloy
X-ray diffraction

ABSTRACT

The 773 K isothermal section of the phase diagram of the Ho–Co–Fe ternary system was investigated by using X-ray diffraction technique, metallographic analysis and scanning electron microscopy with energy dispersive analysis. The isothermal section of the ternary system consists of 6 three-phase regions, 16 two-phase regions and 11 single-phase regions. Three pairs of corresponding compounds of Ho–Co and Ho–Fe systems, i.e., Ho_2Co_{17} and Ho_2Fe_{17}, $HoCo_3$ and $HoFe_3$, $HoCo_2$ and $HoFe_2$, form a continuous series of solid solution. At 773 K the compound $Ho_6Fe_{23-x}Co_x$ was found to have a wide homogeneity range from 0 to 29 at.% Co. The maximum solid solubilities of Fe in Co, Ho_2Co_7, $Ho_{12}Co_7$ and Ho_3Co were determined to be about 10, 9, 2 and 5 at.% Fe, respectively. The maximum solid solubility of Co in Fe is found to be 78 at.% Co.

© 2010 Elsevier B.V. All rights reserved.

1. Introduction

Rare-earth transition-metal antimonides have been extensively examined because of their diverse structures and properties [1]. Some phase diagrams of Ho–Fe–M [2–5] (M = transition metal) and R–Fe–Co (R = rare earth) ternary systems [6–8] have been reported. It was found that only limited investigations on the phase diagrams of ternary Ho–Co–M systems in the whole concentration range are available in literature [9–11]. However, studies on the Ho–Co–Fe ternary system were not found in references. Refs. [12–16] report the investigations on the phase diagrams of the Ho–Co, Ho–Fe and Fe–Co binary systems. There are eight binary compounds in the Ho–Co binary system and four binary compounds in the Ho–Fe system, respectively [9–16]. No binary compound was reported in the Fe–Co binary system [14,16]. The crystallographic data for the binary compounds in the Ho–Co–Fe ternary system can be found in Ref. [17]. The purpose of this work is to investigate the phase relations of the Ho–Co–Fe ternary system by means of experimental methods.

2. Experimental details

Samples with 2 g each were prepared by arc-melting of initial materials of at least of 99.9 wt.% purity under high-purity argon atmosphere. The samples were turned over and remelted three times to ensure good homogeneity. The homogenizing annealing was carried out at elevate temperature for 30 days in an evacuated quartz tube, and then cooled down slowly to 773 K and kept for 10 days. Finally, the samples were quenched into liquid nitrogen. The samples were broken into two parts. One part of the samples were ground into powder and annealed in an evacuated small quartz tube at 773 K for 2 days, then quenched into liquid nitrogen. For the microstructural analysis and metallographic analysis of the samples, standard techniques were used. The metallographic samples were etched by clean water.

Powder diffraction data of all the samples were obtained by using a Rigaku D/max 2500 V diffractometer with a CuK_α radiation and graphite monochromator operated at 40 kV, 200 mA. Phase analysis of the samples was performed by using computer software JADE5.0 [18] applied to the JCPDS-ICDD Powder Diffraction File (PDF) database (ICDD, 2002 release). Scanning electron microscopy (SEM, Hitachi S-3400N) with energy dispersive analysis (EDS, EDAX) and optical microscopy were used for microstructural analysis.

3. Results and discussion

3.1. Phase analysis and solid solubility

Seven binary compounds in the Ho–Co system (Ho_2Co_{17}, Ho_2Co_7, $HoCo_3$, $HoCo_2$, Ho_4Co_3, $Ho_{12}Co_7$, Ho_3Co and four binary compounds in the Ho–Fe system (Ho_2Fe_{17}, Ho_6Fe_{23}, $HoFe_3$, $HoFe_2$) have been confirmed to exist in our binary and ternary alloy samples except $HoCo_5$ at 773 K. The XRD patterns of these compounds basically corresponded with the respective PDF data or the diffraction patterns calculated from the crystallographic data available in literature by using the PowderCell program [19] or lazy program. The compound $HoCo_5$ was considered as high temperature phase with approximate eutectoid decomposition temperature of 1423 K and, below 1423 K, $HoCo_5$ decomposes into the two phases of Ho_2Co_{17} and Ho_2Co_7 [11,12,20]. At 773 K, the samples with compositions near $HoCo_5$ were found to consist of the two phases of $Ho_2Co_{17-x}Fe_x$ and $Ho_2Co_{7-x}Fe_x$. The binary compound $HoCo_5$ was

* Corresponding author. Tel.: +86 771 327 5918; fax: +86 771 323 9406.
E-mail addresses: elsawh@126.com, wei_he@gxu.edu.cn (W. He).

0925-8388/$ – see front matter © 2010 Elsevier B.V. All rights reserved.
doi:10.1016/j.jallcom.2010.09.121

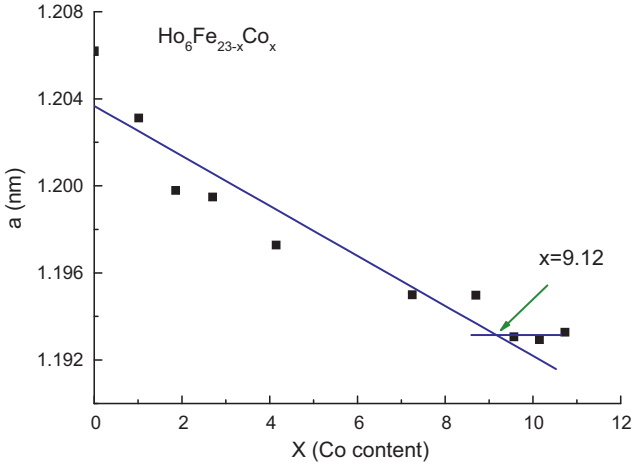

Fig. 1. The variation of the lattice parameters of the compounds $Ho_6Fe_{23-x}Co_x$ with the content of Co.

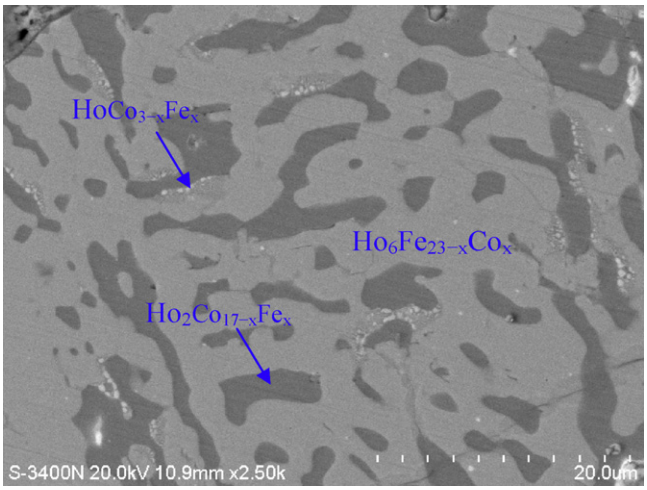

Fig. 2. Micrograph of the sample No. 69 ($Ho_{20.7}Co_{30}Fe_{49.3}$).

not observed under our experimental conditions, which is well agreed with Refs. [11,12,20]. No ternary compound was found in all ternary alloy samples.

It was found that three pairs of corresponding compounds of Ho–Co and Ho–Fe, i.e., Ho_2Co_{17} and Ho_2Fe_{17}, $HoCo_3$ and $HoFe_3$, $HoCo_2$ and $HoFe_2$, form a continuous series of solid solution. This is because these pairs of compounds have the same space groups and crystal structure-types, close lattice parameters and similar characters [17].

The solid solubility of Co in Fe and Ho_6Fe_{23} or Fe in Co, Ho_2Co_7 and Ho_3Co were determined by X-ray diffraction technique using the phase disappearing method combined with scanning electron microscopy with energy dispersive analysis. By comparing the movement and the disappearance of the diffraction patterns of the single phases, the solid solubility of Co or Fe in these compounds were roughly obtained.

The X-ray analysis pointed out that the compound $Ho_6Fe_{23-x}Co_x$ has a wide solid solubility range from around 0 to 30 at.% Co with $x = 0$–8.7. The variation of the lattice parameters of the compounds $Ho_6Fe_{23-x}Co_x$ with the content of Co from 0 to 35 at.% Co (with $x = 0$–10.15) pointing to the solid solution $Ho_6Fe_{23-x}Co_x$ existing with $x = 0$–9.12 (i.e. from 0 to 31 at.% Co), as shown in Fig. 1. However, the sample No.69 with composition of $Ho_{20.7}Co_{30}Fe_{49.3}$ contained the three phases of $Ho_6Fe_{23-x}Co_x$, $Ho_2Co_{17-x}Fe_x$ and $HoCo_{3-x}Fe_x$ indicated that the maximum solid solubility of Co in Ho_6Fe_{23} is no more than 30 at.% Co. Further analysis by the SEM (EDS) also showed that the maximum solid solubility of Co in Ho_6Fe_{23} is about 29 at.% Co. Fig. 2 presents the SEM micrograph of the sample No. 69 ($Ho_{20.7}Co_{30}Fe_{49.3}$) with measured composition of $Ho_{19.4}Co_{29.5}Fe_{51.1}$. The light gray phase with measured composition of $Ho_{21.6}Co_{29.8}Fe_{48.6}$ is $Ho_6Fe_{23-x}Co_x$ ($x = 8.4$), the dark gray phase is $Ho_2Co_{17-x}Fe_x$ ($x = 10.70$) and the white small dots with measured composition of $Ho_{27.7}Co_{28.2}Fe_{44.1}$ are $HoCo_{3-x}Fe_x$ ($x = 1.64$). Therefore, at 773 K, the solid solubility range of the solid solution

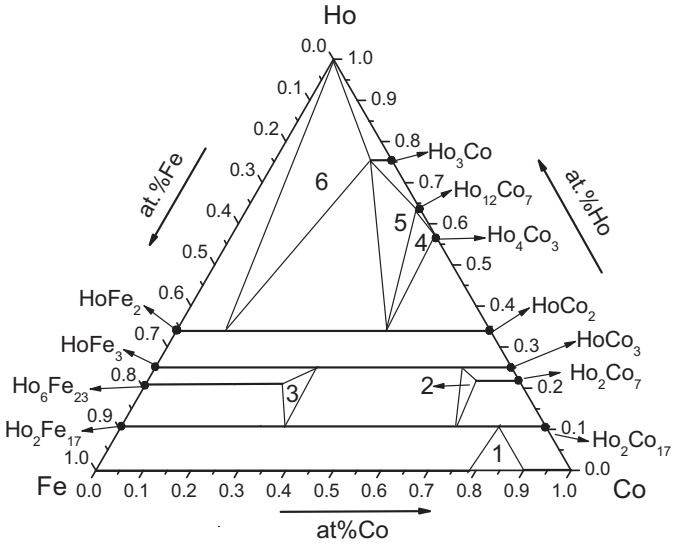

Fig. 3. Isothermal section of Ho–Co–Fe system at 773 K.

$Ho_6Fe_{23-x}Co_x$ was measured to be $0 \le x \le 8.4$, i.e. the maximum solid solubility of Co in $Ho_6Fe_{23-x}Co_x$ is about 29 at.% Co.

Similarly, at 773 K, the maximum solubilities of Fe in Co, Ho_2Co_7, $Ho_{12}Co_7$ and Ho_3Co were determined to be about 10, 9, 2 and 5 at.% Fe, respectively. The maximum solid solubility of Co in Fe was found to be 78 at.% Co. No solid solubility of Fe in Ho_4Co_3 was observed at 773 K.

3.2. Isothermal section at 773 K

The isothermal section of the Ho–Co–Fe ternary system at 773 K was investigated by using X-ray diffraction technique, scanning

Table 1
Details of three phase-regions in the Ho–Fe–Co ternary system.

Phase regions	Phase components	Typical alloy compositions
1	$\alpha Fe_{1-x}Co_x$ ($x = 0.78$) + $\alpha Co_{1-x}Fe_x$ ($x = 0.1$) + $Ho_2Co_{17-x}Fe_x$ ($x = 1.9$)	No. 7 ($Ho_{5.7}Co_{82}Fe_{12.3}$) No. 145 ($Ho_8Co_{81}Fe_{11}$)
2	$Ho_2Co_{17-x}Fe_x$ ($x = 3.42$) + $Ho_2Co_{7-x}Fe_x$ ($x = 0.81$) + $HoCo_{3-x}Fe_x$ ($x = 0.4$)	No. 64 ($Ho_{22.2}Co_{68.0}Fe_{9.8}$)[a] No. 134 ($Ho_{20}Co_{69}Fe_{11}$)[a]
3	$Ho_2Co_{17-x}Fe_x$ ($x = 10.70$) + $Ho_6Fe_{23-x}Co_x$ ($x = 8.4$) + $HoCo_{3-x}Fe_x$ ($x = 1.64$)	No. 69 ($Ho_{20.7}Co_{30}Fe_{49.3}$)[a] No. 156 ($Ho_{20.7}Co_{33}Fe_{46.3}$)[a]
4	Ho_4Co_3 + $HoCo_{2-x}Fe_x$ ($x = 0.66$) + $Ho_{12}Co_{7-x}Fe_x$ ($x = 0.38$)	No. 74 ($Ho_{57.1}Co_{40}Fe_{2.9}$)
5	$Ho_{12}Co_{7-x}Fe_x$ ($x = 0.38$) + $HoCo_{2-x}Fe_x$ ($x = 0.66$) + $Ho_3Co_{1-x}Fe_x$ ($x = 0.2$)	No. 76 ($Ho_{57}Co_{35}Fe_8$) [a] No. 115 ($Ho_{63.3}Co_{32.8}Fe_{3.9}$)
6	Ho + $HoCo_{2-x}Fe_x$ ($x = 1.68$) + $Ho_3Co_{1-x}Fe_x$ ($x = 0.2$)	No. 50 ($Ho_{74.5}Co_{5.5}Fe_{20}$) No. 118 ($Co_{17}Ho_{75}Fe_8$)

[a] Phase identification by XRD and SEM, otherwise by XRD.

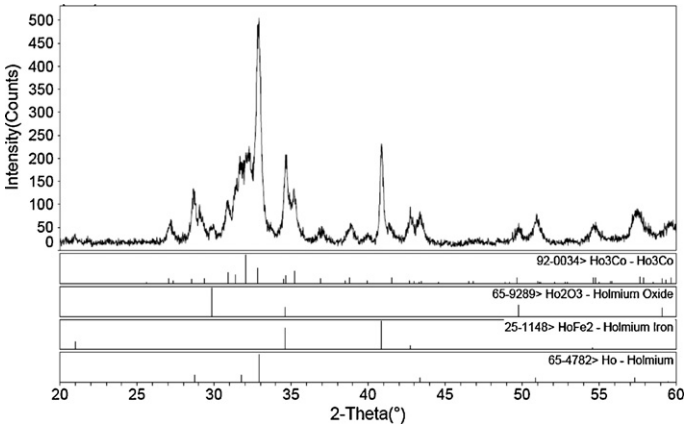

Fig. 4. X-ray diffraction pattern of sample No. 50 ($Ho_{74.5}Co_{5.5}Fe_{20}$).

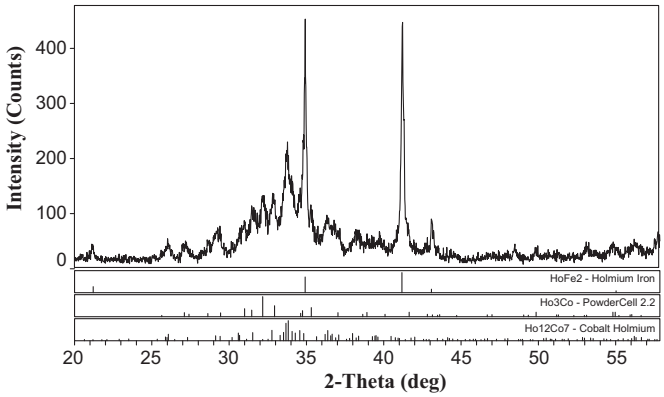

Fig. 5. X-ray diffraction pattern of sample No. 76 ($Ho_{57}Co_{35}Fe_8$).

electron microscopy and metallographic analysis. By comparing and analyzing a total of 164 alloy samples and identifying the phases in each sample, the 773 K isothermal section of the phase diagram of the Ho–Co–Fe ternary system is obtained. The isothermal section, as shown in Fig. 3, consists of 11 single-phase regions, 16 two-phase regions and 6 three-phase regions. Typical alloy composition and details of the three-phase region are given in Table 1. Fig. 4 is the X-ray diffraction pattern of sample No. 50 ($Ho_{74.5}Co_{5.5}Fe_{20}$) located in the three-phase region of $Ho + HoCo_{2-x}Fe_x$ ($x = 1.68$) + $Ho_3Co_{1-x}Fe_x$ ($x = 0.2$). Fig. 5 presents the X-ray diffraction pattern of sample No. 76 ($Ho_{57}Co_{35}Fe_8$) containing the three phases of $Ho_{12}Co_{7-x}Fe_x$, $HoCo_{2-x}Fe_x$ and $Ho_3Co_{1-x}Fe_x$ indicating the existence of the three-phase region of $Ho_{12}Co_{7-x}Fe_x$ ($x = 0.38$) + $HoCo_{2-x}Fe_x$ ($x = 0.66$) + $Ho_3Co_{1-x}Fe_x$ ($x = 0.2$). The SEM metallographic graph of the same sample No. 76 ($Ho_{57}Co_{35}Fe_8$) is given in Fig. 6. The gray background with

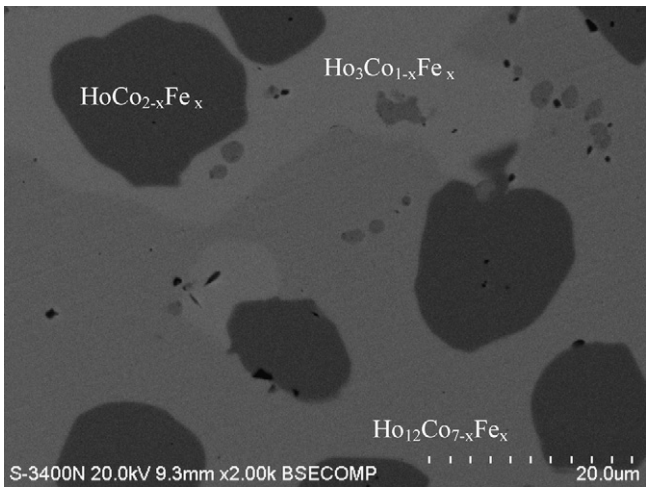

Fig. 6. Metallographic graph of sample No. 76 ($Ho_{57}Co_{35}Fe_8$). The gray background is the phase $Ho_{12}Co_{7-x}Fe_x$, the dark pieces are $HoCo_{2-x}Fe_x$ and the light gray areas are $Ho_3Co_{1-x}Fe_x$.

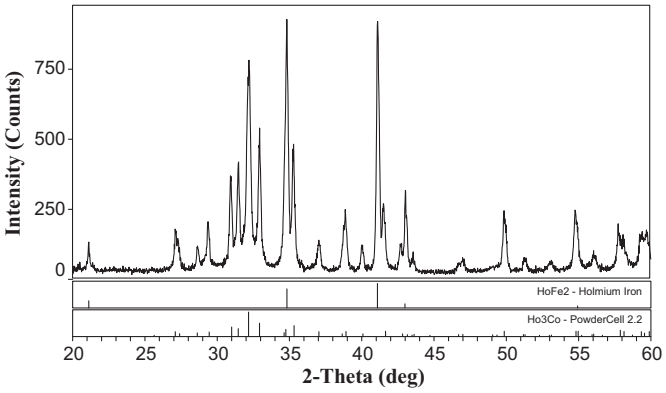

Fig. 7. X-ray diffraction pattern of sample No. 52 ($Ho_{60}Co_{26.5}Fe_{13.5}$).

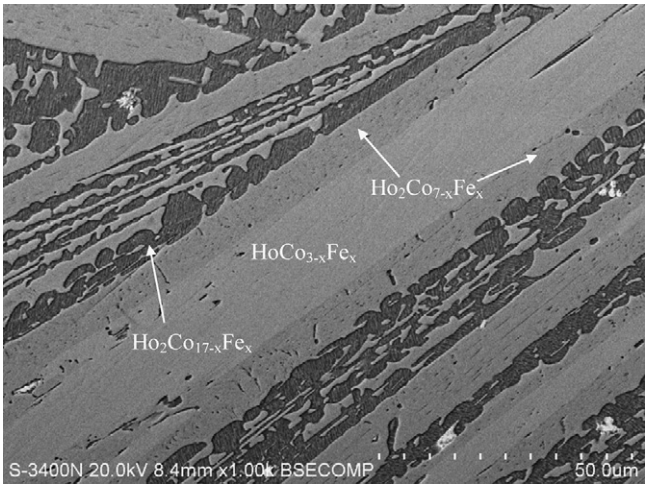

Fig. 8. Metallographic graph of sample No. 134 ($Ho_{20}Co_{69}Fe_{11}$) in the three-phase region of $Ho_2Co_{17-x}Fe_x + Ho_2Co_{7-x}Fe_x + HoCo_{3-x}Fe_x$. The gray area is the phase of $Ho_2Co_{7-x}Fe_x$, the light white-gray area is $HoCo_{3-x}Fe_x$ and the black areas are $Ho_2Co_{17-x}Fe_x$.

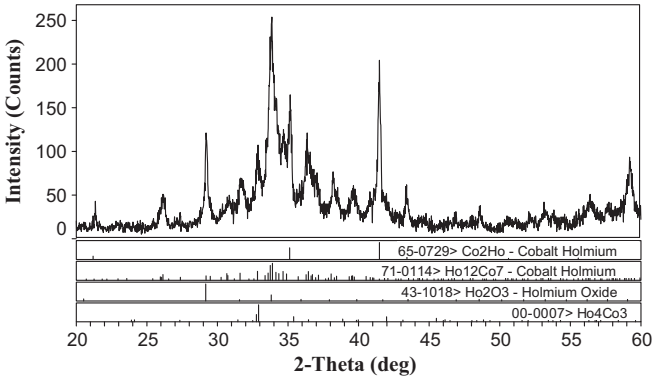

Fig. 9. XRD patterns of No. 74 ($Ho_{57.1}Co_{40}Fe_{2.9}$) consisting of $HoCo_{2-x}Fe_x$, $Ho_{12}Co_{7-x}Fe_x$ and Ho_4Co_3.

composition of $Ho_{61.51}Co_{36.2}Fe_{2.217}$ is the phase $Ho_{12}Co_{7-x}Fe_x$, the dark pieces ($Ho_{33.2}Co_{41.1}Fe_{25.7}$) are $HoCo_{2-x}Fe_x$ and the light gray areas are $Ho_3Co_{1-x}Fe_x$. Fig. 7 presents the X-ray diffraction pattern of sample No. 52 ($Ho_{60}Co_{26.5}Fe_{13.5}$) in the two-phase region of $HoCo_{2-x}Fe_x + Ho_3Co_{1-x}Fe_x$. Fig. 8 is the SEM metallographic graph of sample No. 134 ($Ho_{20}Co_{69}Fe_{11}$) containing three phases of $Ho_2Co_{17-x}Fe_x$ ($x = 3.42$) + $Ho_2Co_{7-x}Fe_x$ ($x = 0.81$) + $HoCo_{3-x}Fe_x$ ($x = 0.4$). The gray area with measured composition of $Ho_{21.73}Co_{67.48}Fe_{10.78}$ is the phase of $Ho_2Co_{7-x}Fe_x$, the light white-gray area ($Ho_{25.53}Co_{65.96}Fe_{8.51}$) is $HoCo_{3-x}Fe_x$ and the black areas are $Ho_2Co_{17-x}Fe_x$. Fig. 9 presents XRD patterns of No. 74 ($Ho_{57.1}Co_{40}Fe_{2.9}$) consisting of $Ho_{12}Co_{7-x}Fe_x$ ($x = 0.38$), $HoCo_{2-x}Fe_x$ ($x = 0.66$) and Ho_4Co_3.

4. Conclusion

The 773 K isothermal section of the phase diagram of the Ho–Co–Fe ternary system was investigated by using X-ray diffraction technique, metallographic analysis, scanning electron microscopy with energy dispersive analysis. The isothermal section of ternary system consists of 6 three-phase regions, 16 two-phase regions and 11 single-phase regions. Three pairs of corresponding compounds of Ho–Co and Ho–Fe, i.e., Ho_2Co_{17} and Ho_2Fe_{17}, $HoCo_3$ and $HoFe_3$, $HoCo_2$ and $HoFe_2$, form a continuous series of solid solution. At 773 K the compound $Ho_6Fe_{23-x}Co_x$ was found to have a wide solubility range from 0 to 29 at.% Co with $x = 0$ –8.4. The maximum solid solubility of Fe in Co, Ho_2Co_7, $Ho_{12}Co_7$ and Ho_3Co were determined to be about 10, 9, 2 and 5 at.% Fe, respectively. The maximum solid solubility of Co in Fe was found to be 78 at.% Fe. No solid solubility of Fe in Ho_4Co_3 was observed at 773 K. No ternary compound was found in all ternary alloy samples.

Acknowledgements

This work was supported by the Natural Science Foundation of China (nos. 50861005 and 50961002) and the Special Foundation for the New Century Ten Hundred Thousand Talents Program of Guangxi (no. 2007217).

References

[1] O.L. Sologub, P.S. Salamakha, in: K.A. Gschneidner Jr., J-C.G. Bunzli, V.K. Pecharsky (Eds.), Handbook on the physics and chemistry of rare earths, 33, Amsterdam, Elsevier, 2003, pp. 35–146.
[2] L.M. Zeng, H.Q. Zhao, J. Alloys Compd. 366 (2004) 201–204.
[3] J.Q. Liu, X.L. Qu, Y.H. Zhuang, J. Alloys Compd. 241 (1996) 196–198.
[4] L.P. Zhang, K.W. Zhou, S.W. Wu, Y.H. Zhuang, J. Alloys Compd. 287 (1999) 195–196.
[5] Y.H. Zhuang, W. Qin, H.Y. Zhou, J. Alloys Compd. 248 (1997) 206–208.
[6] N. Kamiya, T. Sakai, R. Kainuma, I. Ohnuma, K. Ishida, Intermetallics 12 (2004) 417–423.
[7] R. Ducher, R. Kainuma, I. Ohnuma, K. Ishida, J. Alloys Compd. 437 (2007) 93–101.
[8] P. Amornpitoksuk, H. Li, J.-C. Tedenac, S.G. Fries, D. Ravot, Intermetallics 15 (2007) 475–478.
[9] A.V. Tkachuk, H. Bie, A. Mar, Intermetallics 16 (2008) 1185–1189.
[10] V. Raghavan, JPEDAV 28 (2007) 401.
[11] J.Q. Liu, M.Q. Tang, X.Q. Li, J. Alloys Compd. 481 (2009) 161–166.
[12] S. Jin, J. Wang, L.G. Zhang, H.S. Liu, L.B. Liu, F. Zheng, Z.P. Jin, J. Alloys Compd. 477 (2009) 233–238.
[13] G.J. Roe, T.J. OKeefe, Metall. Trans. 1 (1970) 2565–2568.
[14] I. Ohnuma, H. Enoki, O. Ikeda, R. Kainuma, H. Ohtani, B. Sundman, K. Ishida, Acta Mater. 50 (2002) 379.
[15] R. Salamkha, M. Konyk, O. Sologub, O. Bodak, J. Alloys Compd. 234 (1996) 151–156.
[16] J. Huang, H. Zhong, X. Xia, W. He, J. Zhu, J. Deng, Y. Zhuang, J. Alloys Compd. 471 (2009) 74–77.
[17] P. Villars, Pearson's Handbook of Crystallographic Data, Materials Park, OH, 1997.
[18] Jade 5.0, XRD Pattern Processing Materials Data Inc., 1999.
[19] W. Kraus, G. Nolze, J. Appl. Crystallogr. 29 (1996) 301–303.
[20] K.H.J. Buschow, A. Svander Goot, J. Less-Common Met. 19 (1969) 153–158.